Available online at www.sciencedirect.com
SCIENCE DIRECT®
Computer Physics Communications 155 (2003) 77–91
Computer Physics Communications
www.elsevier.com/locate/cpc

Characterizing the spatiotemporal dynamics of turbulence

Shuguang Guan [a], C.-H. Lai [b], G.W. Wei [c,*]

[a] *Department of Computational Science, National University of Singapore, Singapore 117543*
[b] *Department of Physics, National University of Singapore, Singapore 117543*
[c] *Department of Mathematics, Michigan State University, East Lansing, MI 48824, USA*

Received 5 March 2003; received in revised form 30 May 2003

Abstract

This paper introduces a new wavelet-based approach for characterizing the dynamics of turbulence. The proposed approach reduces the dynamics of turbulence into a number of time series, each at a different spatial scale. The effectiveness of the proposed method is illustrated by freely decaying two-dimensional turbulence, which shows three distinct dynamic stages in the present wavelet representation. Increase of the wavelet energies in the large scale subbands characterizes the inverse energy transfer. Moreover, an anomalous transfer of the subband energy and enstrophy among spatial scales is observed during the transient stage. The decaying of the subscale enstrophies exhibits power law scaling and, interestingly, the decay rates increase monotonically with the refinement of the scales.

PACS: 47.32.Cc; 67.40.Fd; 67.40.Vs

1. Introduction

Turbulence is ubiquitous in nature and it inherently involves huge number of degrees of freedom and a wide range of spatial scales. The unsteady feature of turbulence has considerably hindered its understanding. Traditionally, turbulent motion has been studied by Fourier analysis. Our intuition about large and small turbulent scales, and the cascade processes are substantially biased by the Fourier analysis. Other important descriptions, such as Kolmogorov dimensional arguments, also strongly depend on the Fourier spectral distribution. However, Fourier analysis has its limitation for turbulent features of finite spatial or time extensions, and for time-varying unsteady turbulent fields.

Recently, wavelet analysis has been introduced as a powerful tool for studying physical systems that are of unsteady and/or multiscale in nature. Mathematically, wavelets are sets of L^2 functions derived from a single function by two elementary operations: translation and dilation. The most appealing feature of wavelets is that they are simultaneously localized in both physical and spectral spaces. Another important feature is the wavelet multiresolution analysis. Therefore, compared to the usual orthogonal L^2 bases, wavelet bases have much better

* Corresponding author.
E-mail address: wei@math.msu.edu (G.W. Wei).

0010-4655/$ – see front matter
doi:10.1016/S0010-4655(03)00296-0

properties for representing physical signals of unsteady and multiscale nature. Physically, the wavelet transform can decompose a signal into different frequency subbands or scales so that each component can be studied with a resolution matched to its scale, providing excellent frequency and spatial resolution as well as achieving high computational efficiency. So far, wavelet methods have been successfully applied in analyzing, modeling and computing turbulence [1]. For example, the wavelet transform has been used to analyze experimental data of turbulence [2,3]. The local wavelet spectrum was defined based on the orthonormal multiscale wavelet transform, which enables us to study the turbulent flow simultaneously in both physical and spectral spaces [4]. An algorithm based on wavelet-packet transform has been developed to investigate the temporal scaling behaviors of two-dimensional (2D) turbulence [5]. In addition, the nonlinear energy transfer in turbulence has been represented and studied in the wavelet space [6–8]. Recently, an adaptive wavelet approach has been employed for extracting active coherent vortices from the passive background, and for computing the freely decaying turbulence [9–11]. The above-mentioned approaches are the state of art wavelet algorithms and they have significantly enhanced our understanding of turbulence. However, the use of wavelets in all the above-mentioned work focuses either on the analysis of a spatial "pattern", or on a given time series collected at a single spatial point of a turbulent field, or on turbulent field compression. The possibility of reducing large turbulence data and characterizing the temporal motion corresponding to different scales has not been exploited. The purpose of the present work is to propose a new wavelet based method that is capable of characterizing the unsteady time evolution of turbulent eddy formation, enstrophy decaying, as well as energy cascade and transfer among different spatial scales.

In order to characterize the dynamics of turbulence, which usually involves a huge set of data especially recorded in high spatial or temporal resolution, it is necessary to reduce the dynamics and extract the most essential dynamic information. In other words, the characterization should provide a reduced representation which is able to capture both the spatial inhomogeneity and the unsteady evolution of the original spatiotemporal dynamics of turbulence. To this end, it is desirable to reduce the dynamics of turbulence in terms of a minimum set of quantitative indices. However, usual dynamics reduction methods, such as the Fourier analysis and Karhunen–Loéve (KL) decomposition, lose their efficiency when a large amount of activated modes need to be tracked in turbulence, due to the interaction of a large number of degrees of freedom, as well as the incompatibility between the decomposition modes and the physical field of interest. In the current study, a new and effective wavelet-based method is developed for characterizing the dynamics of turbulence. The wavelet multiscale analysis is first carried out to decompose a spatiotemporal turbulent field into a sequence of nested wavelet subspaces at a given time. Then based on this wavelet projection, time series which carry the essential dynamical information corresponding to different frequency subbands can be defined so that the time-varying dynamics of certain turbulent quantity can be studied at different spatial scales. Unlike the conventional spectral characterization, which concentrates on the statistical properties of turbulence related to spatial scales, but fails to explicitly provide temporal information (dynamics), the novelty of the present wavelet-based characterization method lies in that it can simultaneously give both the spatial distribution among various scales and the corresponding subscale evolution of certain flow properties, such as the energy and the enstrophy of the turbulence. For example, based on this characterization, the inverse energy transfer in 2D turbulence can be clearly and directly demonstrated in the physical space rather than in the spectral domain. The enstrophy decaying and the associated power law are further investigated in terms of the evolution of subscale enstrophies. In addition, our method can be used to capture the process of individual vortex pair interaction more effectively and accurately than the Fourier mode analysis.

The mathematical formulation of the present method of wavelet characterization is developed in the next section. In Section 3, the proposed method is applied to the freely decaying 2D turbulence. The numerical aspects of turbulence simulation are briefly discussed and the detailed characterization is reported. This paper ends with a conclusion.

2. Wavelet characterization method

In this section, we introduce a wavelet multiresolution framework to characterize the dynamics of turbulence. The theory of multiresolution analysis (MRA) presents a natural framework to construct orthonormal wavelet bases in the L^2 [12–17]. The MRA on $L^2(\mathbf{R}^3)$ consists of a family of nested subspaces

$$\cdots \subset S_{-1} \subset S_0 \subset S_1 \subset \cdots \tag{1}$$

with the limit $S_\infty = L^2(\mathbf{R}^3)$. The space S_0 contains the scaling function ϕ and the space S_m is spanned by the orthonormal basis obtained by the translation and dilation of the scaling function. In general, an orthogonal wavelet basis can be generated from either a scaling function, or a mother wavelet, by the standard translation and dilation technique.

Usually high-dimensional MRA is constructed by the tensor products of the one-dimensional MRA. Let denote by ϕ^i and ψ^i $(i = x, y, z)$ the scaling function and the mother wavelet in the i direction of the one-dimensional MRA. Then the three-dimensional orthonormal wavelet bases for square integrable turbulent fields are constructed as the tensor products of one-dimensional wavelet bases

$$\Psi^{\alpha\beta\gamma}_{m,n_x,n_y,n_z} = \begin{cases} \psi^x_{m,n_x}\psi^y_{m,n_y}\psi^z_{m,n_z}, & \alpha = H,\ \beta = H,\ \gamma = H, \\ \psi^x_{m,n_x}\psi^y_{m,n_y}\phi^z_{m,n_z}, & \alpha = H,\ \beta = H,\ \gamma = L, \\ \quad\vdots & \quad\vdots \\ \phi^x_{m,n_x}\phi^y_{m,n_y}\phi^z_{m,n_z}, & \alpha = L,\ \beta = L,\ \gamma = L, \end{cases} \qquad (m, n_x, n_y, n_z \in Z). \tag{2}$$

Here, L and H respectively resemble "low-frequency" and "high-frequency", emphasizing the different filter properties of the scaling function and the mother wavelet in the spectral space, i.e. the scaling function can be viewed as a low pass filter ($\hat{\phi}(0) = 1$) while the mother wavelet is a high (band) pass filter ($\hat{\psi}(0) = 0$). $\{\Psi^{HHH}_{m,n_x,n_y,n_z}\}$, $\{\Psi^{HHL}_{m,n_x,n_y,n_z}\}, \ldots,$ and $\{\Psi^{LLL}_{m,n_x,n_y,n_z}\}$ are the orthonormal bases spanning the subspaces $S^{HHH}_m, S^{HHL}_m, \ldots$ and S^{LLL}_m, respectively. Subscript m is the scale index of wavelet transform while n_x, n_y and n_z are the position indices in three dimensions, respectively. These wavelet subspaces are related in the three-dimensional MRA as

$$S_{m+1} = S_m \oplus S^{LLH}_m \oplus S^{LHL}_m \oplus \cdots \oplus S^{HHH}_m, \tag{3}$$

where $S_{m+1} = S^{LLL}_{m+1}$ and $S_m = S^{LLL}_m$.

The wavelet multiresolution analysis (WMA) keeps all the information of the original turbulent field since there exists a perfect reconstruction transform from the wavelet coefficients/modes to the original physical field. Thus, there is nothing to gain from the WMA alone when it is used for turbulent analysis, except some multiscale information at a given time. However, time-varying turbulent fields might involve a huge amount of experimental data or simulated data. Therefore, characterizing the time-varying turbulent features with a reduced amount of data is of pressing importance. In order to substantially reduce the spatiotemporal dynamical data, we need certain quantitative indices which only carry the essential dynamical information. Of course, this reduction process will inevitably lose certain information and make the reconstruction from these indices to the original turbulent field impossible. However, as a bonus, it gives prominence to the most important dynamical features. To this end, we define the following projection operators

$$P^{\alpha\beta\gamma}_m = \sum_{n_x,n_y,n_z \in Z} \left|\Psi^{\alpha\beta\gamma}_{m,n_x,n_y,n_z}\right\rangle\left\langle\Psi^{\alpha\beta\gamma}_{m,n_x,n_y,n_z}\right| \quad \alpha, \beta, \gamma \in \{L, H\}, \tag{4}$$

which can project the physical quantity of the turbulent field $f(x, y, z) \in L^2(\mathbf{R}^3)$ onto the wavelet subspaces $S^{LLL}_m, S^{LLH}_m, \ldots,$ and S^{HHH}_m, respectively, i.e.

$$f_m^{\alpha\beta\gamma} = P_m^{\alpha\beta\gamma} |f\rangle = \sum_{n_x,n_y,n_z\in Z} |\Psi_{m,n_x,n_y,n_z}^{\alpha\beta\gamma}\rangle\langle\Psi_{m,n_x,n_y,n_z}^{\alpha\beta\gamma}|f\rangle = \sum_{n_x,n_y,n_z\in Z} d_{m,n_x,n_y,n_z}^{\alpha\beta\gamma} |\Psi_{m,n_x,n_y,n_z}^{\alpha\beta\gamma}\rangle, \tag{5}$$

where $\{d_{m,n_x,n_y,n_z}^{\alpha\beta\gamma}\}$ are the wavelet coefficients/modes and $\alpha, \beta, \gamma \in \{L, H\}$. The basic idea under this projection process is to decompose a physical quantity of the turbulent field according to the spatial frequency subbands. Naturally, we define the index $\| f_m^{\alpha\beta\gamma} \|^2$ as the energy in the wavelet subband $\alpha\beta\gamma$ $(\alpha, \beta, \gamma \in \{L, H\})$ at scale m. Due to the properties of WMA described above, the wavelet subband energy defined here is a characteristic index of spatial complexity for a given turbulent field. Based on this index, the time series of wavelet subband energy $\rho_m^{\alpha\beta\gamma}(t)$, $(\alpha, \beta, \gamma \in \{L, H\})$ at each given scale m can be obtained as

$$\rho_m^{\alpha\beta\gamma}(t) = \left\| f_m^{\alpha\beta\gamma}(t) \right\|^2 = \sum_{n_x,n_y,n_z\in Z} \left| d_{m,n_x,n_y,n_z}^{\alpha\beta\gamma}(t) \right|^2. \tag{6}$$

Due to the orthogonality of the wavelet basis, we have the Parseval relation

$$\left\| f(t) \right\|^2 = \sum_{m\in Z} \sum_{\alpha,\beta,\gamma\in\{L,H\}}{}' \left\| f_m^{\alpha\beta\gamma}(t) \right\|^2, \tag{7}$$

where the summation $\sum'_{\alpha,\beta,\gamma\in\{L,H\}}$ excludes $\alpha = \beta = \gamma = L$. The summation over the three position indices in the definition Eq. (6) reduces the evolution of all the wavelet coefficients/modes in the wavelet space to a few number of time series. Each of these time series is related to a frequency subband, or a spatial scale. Therefore, the time series $\rho_m^{\alpha\beta\gamma}(t)$, $(\alpha, \beta, \gamma \in \{L, H\})$ give a reduced representation of the quantity of interest at different spatial scales. To illustrate the effectiveness of the proposed method for characterizing turbulence, we consider a few important examples in the next section.

3. Turbulence characterization

3.1. Numerical aspects

In this section, we apply the proposed wavelet method to the characterization of turbulence. For simplicity, we focus on freely decaying 2D turbulence [18]. In the framework of direct numerical simulation (DNS), we consider the 2D incompressible Navier–Stocks equations

$$\frac{\partial \mathbf{u}}{\partial t} + \mathbf{u}\cdot\nabla\mathbf{u} = -\nabla p + \frac{1}{\mathrm{Re}}\nabla^2\mathbf{u}, \nabla\cdot\mathbf{u} = 0, \tag{8}$$

where p is the pressure, Re is the Reynolds number and $\mathbf{u} = (u, v)$ is the velocity field vector which has its x- and y-component $u(x, y, t)$ and $v(x, y, t)$, respectively. The flow is bounded in a square domain $[0, 2\pi] \times [0, 2\pi]$ with 512^2 spatial point resolution and periodic boundary conditions in each direction. The Fourier pseudospectral method and the Adams–Bashforth–Crank–Nicolson (ABCN) scheme are employed for the spatial and temporal discretizations, respectively. The validity for such a numerical scheme has been extensively tested [19,20]. In the present computation, we usually choose $\mathrm{Re} = 5000$ or 6000 to generate turbulent dynamics.

For freely decaying 2D turbulence, the initial condition plays an important role in determining the statistical properties as well as the dynamics. In the present simulation, we choose two commonly used initial spectra prescribed in the Fourier domain

$$E(k, 0) \sim k^n \mathrm{e}^{-(k/k_0)^2}, \tag{9}$$

Table 1
Parameters for two typical numerical simulations

Run	Run1	Run2	Run3	Run4
$E_0(k)$	Eq. (9)	Eq. (10)	Eq. (9)	Eq. (10)
n	4	5	4	6
k_0	16	6	10	6
E_0	0.250	0.500	0.402	0.250
Z_0	153	178	98.4	7.22
Δt	2.5×10^{-4}	2.5×10^{-4}	5×10^{-4}	5×10^{-4}
t_t	50	50	50	50
t_c	8.08×10^{-2}	0.237	0.101	0.372
t_t/t_c	619	211	495	134

$E_0(k)$ is the initial energy spectrum; Re is the Reynolds number; E_0 and Z_0 are the initial energy and enstrophy, respectively; Δt is the time step; t_t is the total integration time; $t_c = 1/\sqrt{Z_0}$ is the initial eddy turnover time.

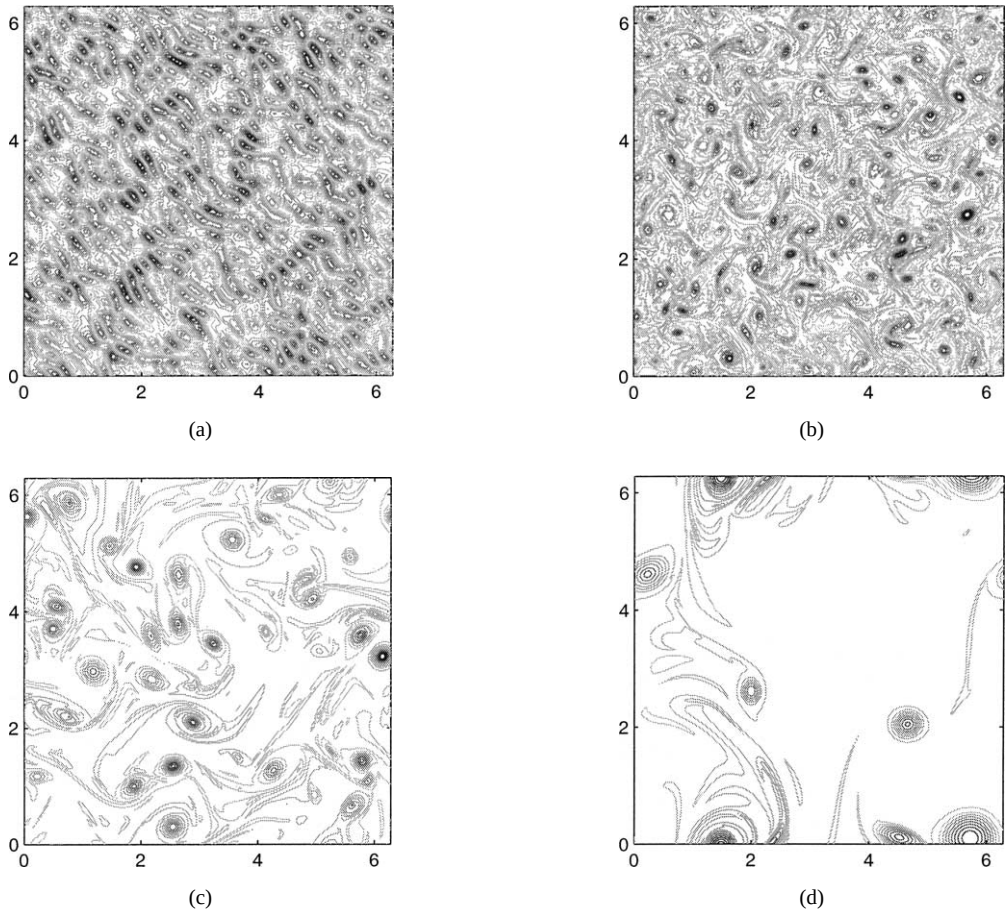

Fig. 1. Vorticity contours of Run1. (a) $t = 0$; (b) $t = 2$; (c) $t = 10$; (d) $t = 50$.

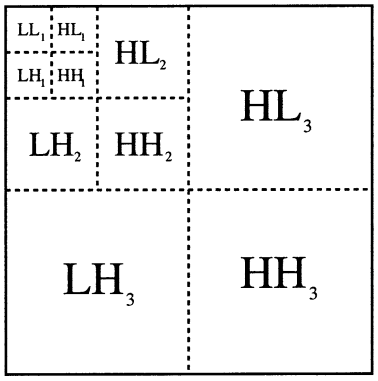

Fig. 2. A schematic plot of two-dimensional three-scale wavelet transform.

or

$$E(k,0) \sim k/\left[1+(k/k_0)^{n+1}\right]. \tag{10}$$

Here k_0 is an adjustable constant. Table 1 summarizes the parameters for the typical tests performed in our simulations. Similar parameters have been considered by many researchers [20–27]. The convergence of the present result has been carefully verified and many other parameters are used to confirm the present findings. The total integration length is 50, which corresponds to several hundreds of initial eddy turnover time. Important features of 2D turbulent dynamics include the formation, interaction and evolution of coherent vortices [24], which can be organized from the disordered background. Typically, coherent vortices are dynamically stable with lifetime longer than the characteristic time scale of the nonlinear turbulent interactions, such as the inertial eddy turnover time [18] (see Fig. 1).

3.2. Wavelet multiscale analysis

A physical quantity of 2D turbulent field can be regarded as a 2D pattern or a 2D image from the point of view of image processing. Fig. 2 shows the typical 2D multiscale wavelet decomposition to such a quantity. The Daubechies-8 wavelets are used in the present WMA. Nevertheless, the results are generally independent of the wavelet used. In Fig. 2, the upper left square labeled by LL_1 contains the information of the largest spatial scale in both the horizontal and vertical directions. Correspondingly, other nine regions contain information in different high frequency subbands (or small scales). Among them, the three diagonal regions labeled by HH_3, HH_2, and HH_1 correspond to the highest frequency subbands at each scale and they contain the most detailed information of the original turbulent field in the corresponding scale. WMA of a typical turbulent vorticity field is illustrated in Fig. 3. This turbulent field includes both the coherent components and the highly oscillatory components as shown in Fig. 3(a). For the purpose of visualization, we plot the decomposed states in physical space. For instance, the vorticity field shown in Fig. 3(b) is reconstructed from the wavelet modes of wavelet subspace LL_1. Similarly, Figs. 3(c)–3(e) correspond to turbulent states projected into the wavelet subbands HH_1, HH_2 and HH_3, respectively. It is seen that Fig. 3(b) mainly contains the coherent part of the turbulent field, while high-frequency subbands, as shown in Figs. 3(c)–3(e), consist of large gradients. Although there exists certain similarity among Figs. 3(c)–3(e), the energy spectra in Fig. 3(f) confirm that they belong to different frequency subbands.

3.3. Wavelet characterization of the energy evolution

The major concern of the present paper is to characterize the temporal evolution of the turbulent field at a number of spatial scales. One interesting dynamical feature of 2D turbulence is the inverse energy transfer. To

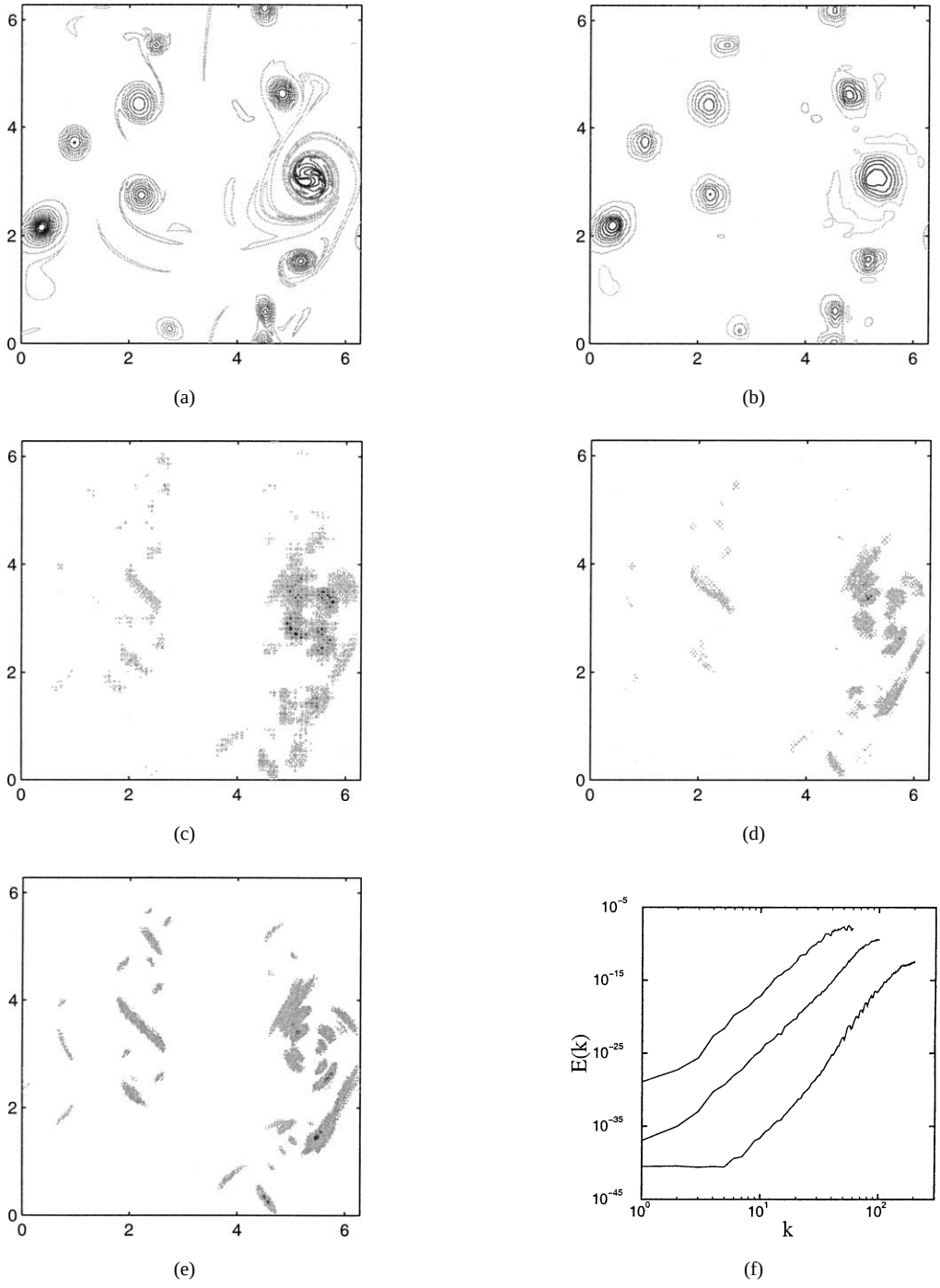

Fig. 3. (a) Vorticity contour of Run1 at $t = 35$. (b)–(e) vorticity contours of different components of turbulent state (a) corresponding to wavelet subbands LL_1, HH_1, HH_2 and HH_3, respectively; (f) from left to right: energy spectra of (c), (d) and (e), respectively.

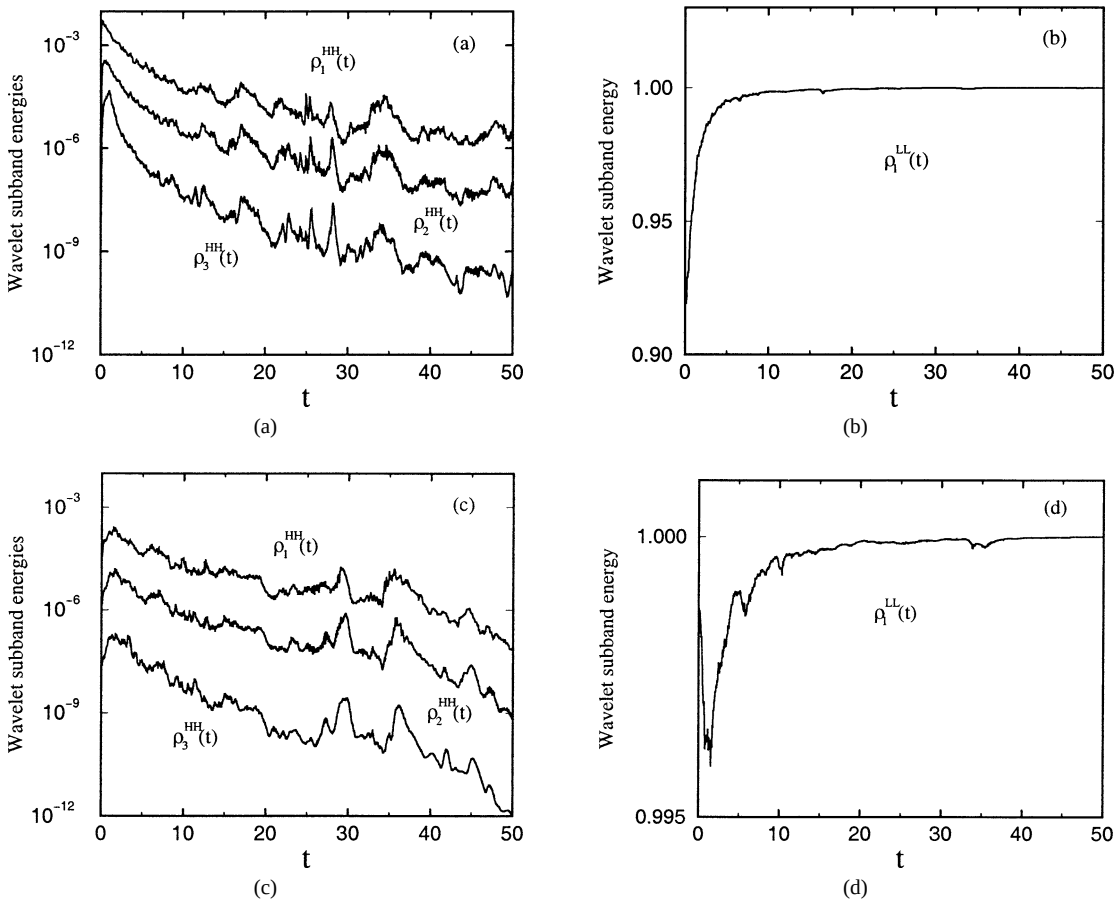

Fig. 4. The wavelet characterization of the dynamics for Run1 ((a) and (b)), and Run2 ((c) and (d)).

characterize this important dynamical feature, it is desirable to simultaneously give both energy distribution among various spatial scales and the corresponding subscale energy evolution. For the incompressible flow, the evolution of the kinetic energy per unit volume, i.e. $\varepsilon(x, y, t) = \mathbf{u}^2/2 = (u^2 + v^2)/2$, obeys the following dynamic equation:

$$\frac{\partial \varepsilon}{\partial t} = -\nabla \cdot \mathbf{u}(\varepsilon + p) + \frac{1}{\mathrm{Re}}\nabla^2 \varepsilon, \tag{11}$$

where the first term $\mathbf{u}(\varepsilon + p)$ is the energy flux due to the transfer of the fluid mass and the last term denotes the kinetic energy dissipation. By means of wavelet projection operators defined in Eq. (4), the turbulent energy field $\varepsilon(x, y, t)$ can be decomposed into a series of wavelet subspaces, corresponding to different spatial scales as shown in Fig. 2. We record the time evolutions of the subscale energies $\rho_m^{\alpha\beta}(t)$ at four typical subbands LL_1, HH_1, HH_2 and HH_3. Here, the wavelet subband energies have been normalized by the total energy $\|\varepsilon(t)\|$ in order to exclude the influence of the energy decaying in 2D turbulence. In principle, information in other spatially anisotropic subbands, such as LH_3 and HL_3, could also be important if the system involves directional inhomogeneity and geometric inhomogeneity.

One advantage of the proposed wavelet method is that it monitors the dynamics of the physical quantity under study at different scales. Two typical dynamics characterized in Fig. 4 by the time series of wavelet subband energies at three high-frequency subbands (HH_m, $m = 1, 2, 3$) and the low-frequency subband (LL_1). Contrary to the usual energy characterization of decaying 2D turbulence, which shows smooth, slow and monotonic decaying, the

wavelet characterization reveals that actually the energy evolutions at high-frequency subbands are highly unsteady and intermittent. In addition, it is found that the time series $\rho_m^{HH}(t)$ $(m = 1, 2, 3)$, as plotted in Fig. 4(a) exhibit similar dynamical features among three high-frequency subbands. On average, there is a dominant decay with respect to time in all small-scales, which implies the formation of large coherent vortices from the random initial field in 2D turbulence. The gradual increase of the energy at the large scale in Fig. 4(b) confirms such vortex formation.

By using the present wavelet characterization, the decaying of the 2D turbulence can be divided into three dynamical stages. The first stage, from $t = 0$ to $t \approx 2$, is a transient period, for which the present wavelet method reveals a subband-dependent anomalous energy transfer. As shown in Fig. 4(a), during this transient period, two high-frequency scales HH_2 and HH_3 actually gain energies. In contrast, there is an energy loss in scale HH_1. As the energy density in the HH_1 scale is much larger than that in HH_2 and HH_3 scales, the net effect in the small scales is the loss of energy. Correspondingly, there is a gain in energy at the large scale LL_1. The above analysis reveals that although in general the energy in 2D turbulence transfers inversely from small scale to large scale, the detailed energy transport among different scales might be quite complicated. At present, we do not have a satisfactory explanation for this complicated energy transfer among different spatial scales. Certain typical small-scale structures, such as vorticity-gradient sheets, might be related to this energy transfer during the initial stage [23]. Figs. 4(c) and 4(d) show results for the second numerical experiment, in which the initial energy peaks at a lower wavenumber and decays fast with respect to the wavenumber, see Table 1. In this case, we found a more typical transient period, in which all high-frequency scales gain certain energies, whereas the low-frequency scale LL_1 loses energy.

The second stage, from $t \approx 2$ to $t \approx 10$ as shown in Fig. 4(a), corresponds to the period of fast vortex formation. During this stage, all high-frequency scales lose energy, while the low-frequency scale gains energy. Although the decrease of energy at small scales and the increase at large scales are not monotonic due to the vortex interactions, their trend is obvious. Figs. 4(a) and 4(c) show different decay rates for the three high-frequency subband energies. Obviously, there is a fast generation, interaction and merger of small size coherent vortices during the stage.

The last stage, after $t \approx 10$, is a period of large vortex dominance. As shown in Figs. 4(b) and 4(d), most energy has been accumulated in the low-frequency scales. Turbulence is dominated by the motion of a few large vortices, see Fig. 1(c). The interaction among the coherent vortices is no longer as frequent as that in earlier times because they are well-separated. However, there is still energy exchange among different spatial scales. At this stage, the vortex dynamics can be described by two basic dynamical processes: the mutual free vortex advection and vortex merger.

Another advantage of the proposed wavelet approach is that it gives detailed characterization of individual vortex pair interaction during the stage of large vortex dominance. As strong intermittency caused by the vortex merger is associated with the transient increase in the palinstrophy, this strong nonlinear interaction is traditionally characterized by a transient peak in the plot of mean wave number $\xi(t) = \sqrt{P(t)/Z(t)}$, as shown in Fig. 5(a). Here, $P(t)$ and $Z(t)$ are the palinstrophy and the enstrophy, respectively. From Fig. 5(a), one can identify a small hump at about $t = 25$, which corresponds to the merger of two interacting vortices, as shown in Figs. 5(b) and 5(c). However, such kind of humps are not obvious enough in this mean wavenumber characterization. In contrast, the present wavelet approach captures the detailed vortex interaction process by an obvious intermittent burst of wavelet subband energy as shown in Fig. 5(d). The energy peaks in high frequency subband faithfully record the narrow vortex filaments formed during the vortex merger. In fact, during the time interval $(20, 30)$, there are three counts of such vortex interacting processes as shown in Fig. 5(d). However, not all of these events can be clearly identified by the mean wave number $\xi(t)$ as in Fig. 5(a). Moreover, the time duration of the vortex merger process can be accurately determined from the half-width of the peak in the plot of $\rho_3^{HH}(t)$.

3.4. Wavelet characterization of the enstrophy decaying

The study of scaling laws is a central issue of turbulence theory. In the conventional spectral domain, the scaling behaviors of turbulence are well manifested by the Kolmogorov cascade scenarios [28]. In 2D turbulence, where

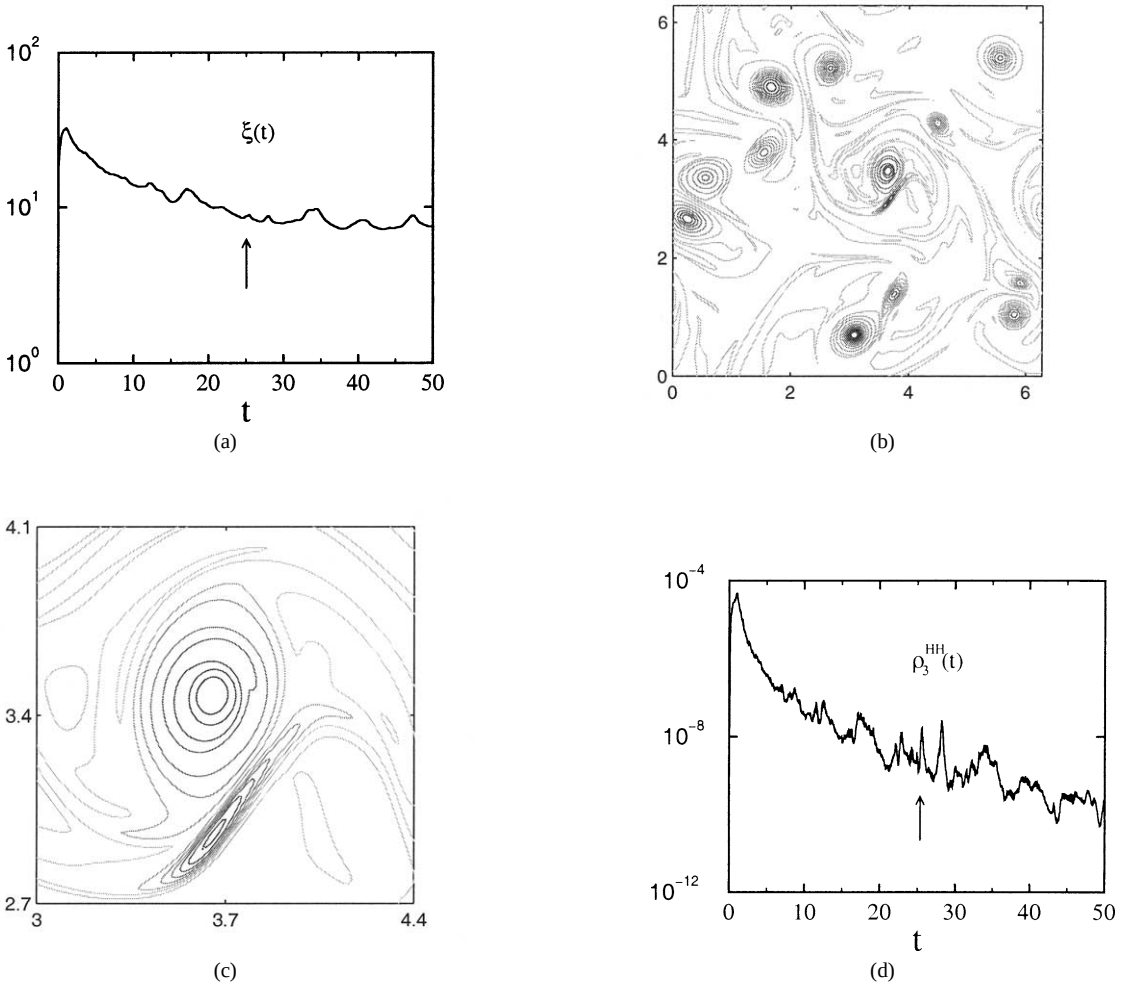

Fig. 5. (a) The mean wavenumber characterization of the vortex dynamics of Run1; (b) vorticity contour showing a typical vortex merger events, which begins at $t = 25$; (c) close-up of (b); (d) the wavelet characterization of the vortex dynamics of Run1.

the energy and the enstrophy are both conserved for the inviscid limit, the Kraichnan–Batchelor theory [18] predicts a direct enstrophy cascade and an inverse energy cascade. Physically, the inverse energy transfer in 2D turbulence corresponds to the formation and evolution of the coherent vortices. It has been further point out that the vortex dynamics also demonstrates the temporal scaling behaviors in the physical space [29–31].

In two-dimensional turbulence, the energy

$$E(t) = \frac{1}{2}\int_{\Omega} \mathbf{u}^2(\mathbf{x}, t)\,\mathrm{d}\mathbf{x}, \tag{12}$$

and the enstrophy, defined as the mean square vorticity,

$$Z(t) = \frac{1}{2}\int_{\Omega} \omega^2(\mathbf{x}, t)\,\mathrm{d}\mathbf{x}, \tag{13}$$

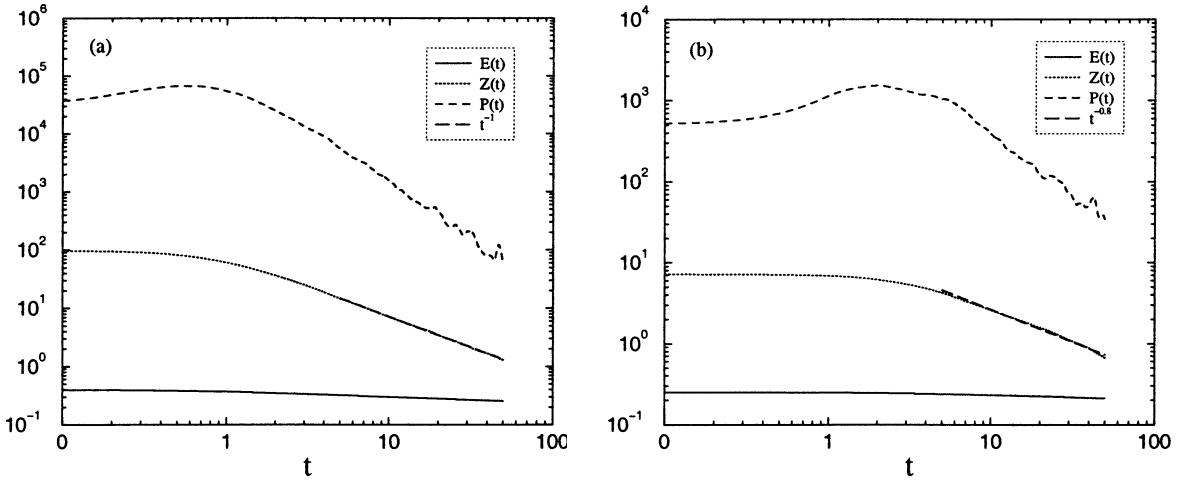

Fig. 6. The evolution of energy E, enstrophy Z and palinstrophy P for (a) Run3 and (b) Run4.

where **u** and ω respectively denote the velocity field vector and the vorticity, are the most important flow properties because they are the only quadratic conserved quantities for the inviscid flow [32]. Therefore, the study of the transfer cascade and the dissipation law of the enstrophy is the key for the understanding of the 2D turbulence. In two-dimensional turbulence with low viscosity, it is observed that the energy is almost conserved while the enstrophy decays significantly. The enstrophy dissipation law derived by Batchelor based on a self-similar analysis [18], predicts that the overall decay of enstrophy satisfies the power laws $Z(t) \sim t^{-2}$. However, the decaying dynamics, especially the enstrophy dissipation law of freely decaying two-dimensional turbulence has not been investigated from the angle of different spatial scales. In the following, we investigate the decaying law of the enstrophies at different spatial scales.

Fig. 6 shows the evolution of the main flow properties for two typical runs listed in Table 1. The evolution of the enstrophy is characterized by the smooth, monotonic and algebraic decaying. After the initial transience, the observed decay rates of the enstrophy are much slower than that of the theoretical prediction. For the present initial conditions, the decay rates of $Z(t)$ are about -1.0 for Run3 and -0.8 for Run4. It is believed that the formation of coherent vortices, as well as their large-scale intermittent dynamics, slow down the turbulence decaying process.

The evolution of the vorticity is governed by the Helmholtz vorticity equation. For the flow in xy plane, it degenerates to a scalar equation

$$\frac{\partial \omega}{\partial t} = -u\frac{\partial \omega}{\partial x} - v\frac{\partial \omega}{\partial y} + \frac{1}{\mathrm{Re}}\nabla^2\omega, \tag{14}$$

where $\omega = \omega_z$ is the vorticity component perpendicular to the flow plane. The vorticity evolution corresponds to a series of two-dimensional patterns. Applying the projection operator defined in Eq. (4) to the vorticity field $\omega(x, y, t)$ and using

$$\sum_{m}^{M} \sum_{\alpha,\beta\in L,H} P_m^{\alpha\beta} = 1 \tag{15}$$

yield the evolution of vorticity in the wavelet space

$$\omega(x, y, t) = \sum_{n_x,n_y} d^{LL}_{1,n_x,n_y}(t)\left|\Psi^{LL}_{1,n_x,n_y}\right\rangle + \sum_{m>1}^{M} {\sum_{\alpha,\beta\in\{L,H\}}}' \sum_{n_x,n_y} d^{\alpha\beta}_{m,n_x,n_y}(t)\left|\Psi^{\alpha\beta}_{m,n_x,n_y}\right\rangle, \tag{16}$$

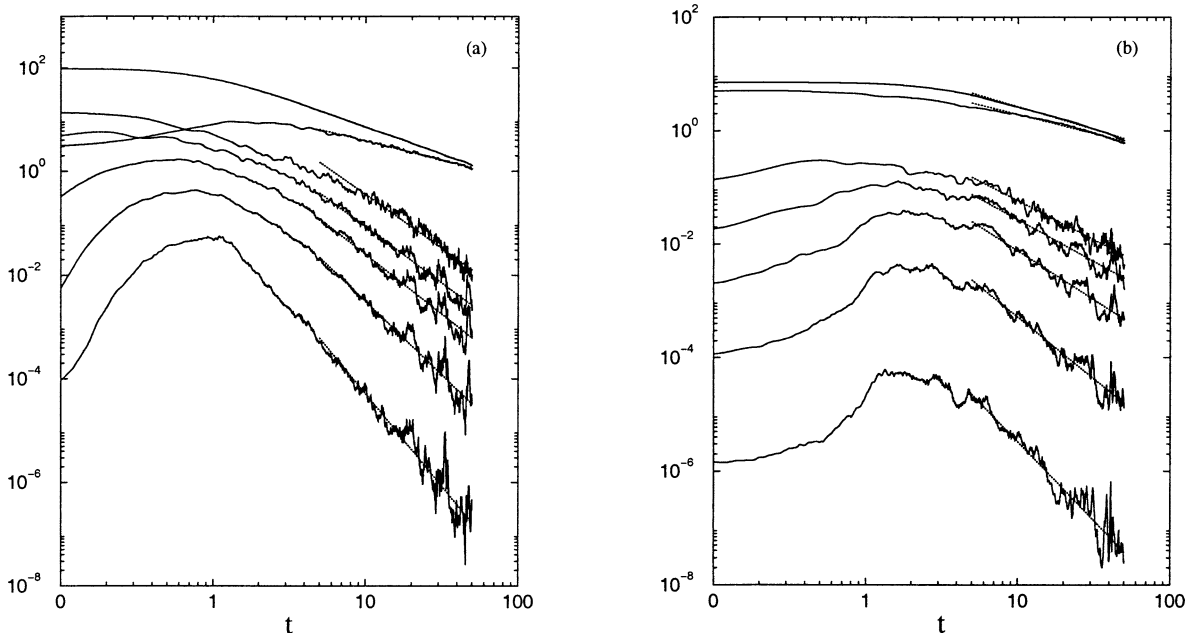

Fig. 7. The power law decay of the subscale enstrophies for Run3 (a) and Run4 (b), respectively. From the up to the bottom: the total enstrophy and the subscale enstrophies at wavelet subbands LL_1, HH_1, HH_2, HH_3, HH_4 and HH_5, respectively. The curves of the total enstrophy coincide the corresponding curves $Z(t)$ in Fig. 6. The dotted lines are the power law fitting ($t \geqslant 5$).

where M denotes M-scale wavelet transform and the summation $\sum'_{\alpha,\beta\in\{L,H\}}$ excludes $\alpha = \beta = L$. With the definition of Eq. (13) and the Parseval relation, we have

$$Z(t) = \sum_{n_x,n_y} \left|d^{LL}_{1,n_x,n_y}(t)\right|^2 + \sum_{m>1}^{M} \sum_{\alpha,\beta\in\{L,H\}}{}' \sum_{n_x,n_y} \left|d^{\alpha\beta}_{m,n_x,n_y}(t)\right|^2. \tag{17}$$

This shows that after the wavelet decomposition, the enstrophy has been projected onto different wavelet frequency subbands, corresponding to different spatial scales. Reasonably, the subscale enstrophy, i.e. the enstrophy in each wavelet frequency subband, can be defined as the total wavelet energy in such subband

$$Z^{\alpha\beta}_m(t) = \sum_{n_x,n_y} \left|d^{\alpha\beta}_{m,n_x,n_y}(t)\right|^2. \tag{18}$$

Physically, the subscale enstrophies are related to the vorticity generated by the turbulent motion at certain spatial scales. With this definition, the total enstrophy evolution can be decomposed as

$$Z(t) = Z^{LL}_1(t) + \sum_{m>1}^{M} \sum_{\alpha,\beta\in\{L,H\}}{}' Z^{\alpha\beta}_m(t). \tag{19}$$

The temporal evolution of the enstrophy can be studied at different spatial scales in terms of the time series of the subscale enstrophies. We carry out five-scale wavelet decomposition of the vorticity field $\omega(x, y, t)$ and record the time series of the subscale enstrophies at the diagonal subbands, i.e. the subbands LL_1, $HH_1, \ldots, HH_5$. Fig. 7 plots the temporal evolution of the subscale enstrophies at these typical subbands. Immediately, several new features of the dynamics of the subscale enstrophies can be revealed. From Fig. 6, the total enstrophy is shown to decay smoothly and monotonically. In Fig. 7, however, it is found that this is no longer the case for the subscale

Table 2
The exponents of power law decaying of the subscale enstrophies. The settings of Run5 is the same as Run4 except Re = 6000

Subband	LL_1	HH_1	HH_2	HH_3	HH_4	HH_5	Total Z
Run3	−0.74	−2.07	−2.17	−2.30	−2.83	−3.57	−1.00
Run4	−0.68	−1.38	−1.48	−1.72	−2.17	−2.77	−0.80
Run5	−0.55	−1.43	−1.73	−2.02	−2.48	−2.93	−0.70

enstrophies. Instead, the enstrophy at large scale (subband LL_1) decays with small oscillations, while the dynamics of enstrophies at small scales (subbands $HH_1, HH_2, \ldots, HH_5$) are highly intermittent though their trends are essentially decaying. It is notable that an anomalous evolution of the subscale enstrophies is observed during the transient stage (roughly $t < 3$). In Fig. 7(a), it is seen that the enstrophies at subbands HH_5, HH_4, HH_3 and LL_1 actually increase instead of decay during the initial period. Similarly, as shown in Fig. 7(b), the subscale enstrophies increase at all the small scale subbands (subbands $HH_1, HH_2, \ldots, HH_5$). Particularly, the gain of enstrophy in the large scale (subband LL_1 in Fig. 7(a)) implies that there exists enstrophy transfer from the small scales to the large ones for certain initial conditions although on average the enstrophy goes from the large scale to the small scale.

After the transience, the time series of the subscale enstrophies clearly show that the turbulence enters into the decaying regime, in which the coherent vortex advection and merger dominate the dynamics. The vortex merger processes lead to the strong intermittent dynamics of the subscale enstrophies, as effectively characterized by the bursts in the small-scale enstrophies in Fig. 7. In spite of these highly intermittent dynamics, the power law decay still holds for the trends of the subscale enstrophies. The exponents of the power law fitting to the subscale enstrophies are listed in Table 2 for the three typical runs. It is found that the smaller the scale, the faster the decaying of the subscale enstrophy. This property is independent of the initial conditions and the total scale of the wavelet decomposition. Moreover, the influence of the Reynolds number to the decaying exponents of subscale enstrophy can be obtained by comparing Run4 and Run5 in Table 2. It is found that with the increase of the Reynolds number, the magnitude of the decaying exponent of the total enstrophy decreases. However, this does not imply the decrease of all the magnitudes of the decaying exponents of the subscale enstrophy. In fact, the magnitude of the decaying exponent of the subscale enstrophy only decreases at large scale (LL_1), while on the contrary, it increases at small scales (HH_i, $i = 1, 2, \ldots, 5$). In two dimension, physically the nonlinear interaction causes the vorticity to cascade toward small scales. Since viscosity acts most strongly on the smaller scales, it turns out that, the enstrophy is nearly conserved inside the large-scale coherent vortices, and can only be effectively dissipated by the formation of small-scale vorticity filaments during the vortex merger [24]. For this reason, one observes faster decaying for the subscale enstrophies at smaller scales.

4. Conclusion

In this paper, a new wavelet method is proposed to characterize the freely decaying turbulence. The goal of the current characterization is to give a reduced representation of the original spatiotemporal turbulent dynamics, and at the mean time to retain the essential dynamical and multiscale information. Wavelet subband energy is defined as the characteristic index based on the multiresolution analysis. Numerical experiments demonstrate that the proposed wavelet method provides a powerful characterization of the dynamics of turbulence.

Using the proposed wavelet method, the dynamics of freely decaying turbulence is divided into three distinct stages, i.e. stages of initial transience, fast vortex formation, and large vortex dominance. Due to this multiscale characterization of the dynamics of 2D turbulence, some new features, such anomalous subband energy and enstrophy transfer are observed. It is shown that the individual vortex pair interaction can also be effectively characterized during the period of large vortex dominance. Further analysis reveals that the decay of the subscale

enstrophies still exhibits scaling behavior and the subscale enstrophy decays faster with respect to the refinement of the spatial scales.

Acknowledgement

The authors thank Mr. Y.C. Zhou for assistance. This work was supported by the National University of Singapore, the Temasek Laboratories at National University of Singapore and the Michigan State University.

References

[1] M. Farge, N.K.-R. Kevlahan, V. Perrier, K. Schneider, in: J.C. Van Den Berg (Ed.), Wavelet in Physics, Cambridge University Press, Cambridge, 1999, p. 117.
[2] F. Argoul, A. Arnéodo, G. Grasseau, Y. Gagne, E.J. Hopfinger, U. Frisch, Wavelet analysis of turbulence reveals the multifractal nature of the Richardson cascade, Nature 338 (1989) 51.
[3] L. Hudgins, C.A. Friehe, M.E. Mayer, Wavelet transforms and atmospheric turbulence, Phys. Rev. Lett. 71 (1993) 3279.
[4] M. Do-Khac, C. Basdevant, V. Perrier, K. Dang-Tran, Wavelet analysis of 2D turbulent fields, Physica D 76 (1994) 252.
[5] A. Siegel, J.B. Weiss, A wavelet-packet census algorithm for calculating vortex statistics, Phys. Fluids 9 (1997) 1988.
[6] C. Meneveau, Analysis of turbulence in the orthonormal wavelet representation, J. Fluid Mech. 232 (1991) 469;
C. Meneveau, Dual spectral and mixed energy cascade of turbulence in the wavelet representation, Phys. Rev. Lett. 66 (1991) 1450.
[7] M. Iima, S. Toh, Wavelet analysis of the energy transfer caused by the convective terms: Application to the Burgers shock, Phys. Rev. E 52 (1995) 6189.
[8] K. Kishida, K. Araki, S. Kishiba, K. Suzuki, Phys. Rev. Lett. 83 (1999) 5487.
[9] J. Fröhlich, K. Schneider, Computation of decaying turbulence in an adaptive wavelet basis, Physica D 134 (1999) 337.
[10] M. Farge, K. Schneider, N. Kevlahan, Non-Gaussianity and coherent vortex simulation for two-dimensional turbulence using an adaptive orthogonal wavelet basis, Phys. Fluids 11 (1999) 2187.
[11] M. Farge, G. Pellegrino, K. Schneider, Coherent vortex extraction in 3D turbulent flows using orthogonal wavelets, Phys. Rev. Lett. 87 (2001) 054501.
[12] Y. Meyer, Wavelets and Operators, in: Cambridge Stud. Adv. Math., Vol. 37, Cambridge Univ. Press, Cambridge, 1992.
[13] I. Daubechies, Orthonormal bases of compactly supported wavelets, Comm. Pure Appl. Math. 41 (1988) 909.
[14] I. Daubechies, Ten Lectures on Wavelets, in: CBMS-NSF Series in Applied Mathematics, SIAM, Philadephia, PA, 1992.
[15] S. Mallat, Multiresolution approximations and wavelet orthonormal bases of $L^2(R)$, Trans. Amer. Math. Soc. 315 (1989) 68.
[16] C.K. Chui, An Introduction to Wavelets, Academic Press, San Diego, 1992.
[17] S. Guan, C.-H. Lai, G.W. Wei, A wavelet method for the characterization of spatiotemporal patterns, Physica D 163 (2002) 49.
[18] R.H. Kraichnan, Inertial ranges in two-dimensional turbulence, Phys. Fluids 10 (1967) 1417;
G.K. Batchelor, Computation of the energy spectrum in homogeneous two-dimensional turbulence, Phys. Fluids (Suppl. II) 12 (1969) 233;
For a review, see R.H. Kraichnan, D. Montgomery, Two-dimensional turbulence, Rep. Prog. Phys. 43 (1980) 547;
M. Lesieur, Turbulence in Fluids, Kluwer Academic, Dordrecht, 1997;
H. Kellay, W. Goldburg, Two-dimensional turbulence: a review of some recent experiments, Rep. Prog. Phys. 65 (2002) 845.
[19] S.Y. Yang, Y.C. Zhou, G.W. Wei, Comparison of the discrete singular convolution algorithm and the Fourier pseudospectral method for solving partial differential equations, Comput. Phys. Commun. 143 (2002) 113.
[20] S. Guan, Y.C. Zhou, G.W. Wei, C.-H. Lai, Controlling flow turbulence, Chaos 13 (2003) 64.
[21] P. Orlandi, Fluid Flow Phenomena, A Numerical Toolkit, Kluwer Academic, Dordrecht, 2000.
[22] S. Kida, Numerical simulation of two-dimensional turbulence with high-symmetry, J. Phys. Soc. Japan. 54 (1985) 2840.
[23] M.E. Brachet, M. Meneguzzi, H. Politano, P.L. Sulem, The dynamics of freely decaying two-dimensional turbulence, J. Fluid Mech. 194 (1988) 333.
[24] J.C. Mcwilliams, The emergence of isolated coherent vortices in turbulent flow, J. Fluid. Mech. 146 (1984) 21;
J.C. Mcwilliams, The vortices of two-dimensional turbulence, J. Fluid. Mech. 219 (1990) 361.
[25] R. Benzi, S. Patarnello, P. Santangelo, On the statistical properties of two-dimensional decaying turbulence, Europhys. Lett. 3 (1987) 811.
[26] W.H. Matthaeus, W.T. Stribling, D. Martinez, S. Oughton, D. Montgomery, Selective decay and coherent vortices in two-dimensional incompressible turbulence, Phys. Rev. Lett. 66 (1991) 2731.
[27] P. Santangelo, R. Benzi, B. Legras, The generation of vortices in high-resolution, two-dimensional decaying turbulence and the influence of initial conditions on the breaking of self-similarity, Phys. Fluids A 1 (1989) 1027.
[28] U. Frisch, Turbulence, Cambridge University Press, Cambridge, 1995.

[29] G.F. Carnevale, J.C. Mcwilliams, Y. Pomeau, J.B. Weiss, W.R. Young, Evolution of vortex statistics in two-dimensional turbulence, Phys. Rev. Lett. 66 (1991) 2735.
[30] R. Benzi, M. Colella, M. Briscolini, P. Santangelo, A simple point vortex model for two-dimensional decaying turbulence, Phys. Fluids A 4 (1992) 1036.
[31] J.B. Weiss, J.C. Mcwilliams, Temporal scaling behavior of decaying two-dimensional turbulence, Phys. Fluids A 5 (1993) 608.
[32] In three-dimensional turbulence, the two conserved quadratic quantity for the Euler flow are the energy and the helicity $\int_\Omega \mathbf{u}\cdot\omega\,\mathrm{d}x$, which measures the swirliness about the local direction of flow. The enstrophy is not a conserved quadratic quantity since it can be amplified by the stretching of the vortex tubes, i.e. increased by the properly oriented velocity gradient. In two dimension, the vortex stretching mechanism is absent because the velocity gradient is always perpendicular to the vorticity. As the consequence, the enstrophy is a constant of motion.